The Spherical Mirror Fabry-Perot Interferometer

Michael Hercher

The theory, design, and use of the confocal spherical mirror Fabry-Perot interferometer (FPS) is described in detail. Topics covered include performance of an FPS for small departures from the confocal mirror separation, optimization of the (resolution) × (light gathering power) product, factors limiting realizable finesse, mode matching considerations, alignment procedures, and general design considerations. Two specific instruments are described. One is a versatile spectrum analyzer with piezo-electric scanning; the other is a highly stable etalon with fixed spacing. Examples of the performance of these instruments are given.

I. Introduction

The spherical mirror Fabry-Perot interferometer (FPS) was first described by Connes over ten years ago.[1-3] Although this instrument is mentioned in some recent texts,[4,5] Connes' papers contain the only detailed descriptions of the spherical mirror Fabry-Perot interferometer. This paper is intended to review and extend Connes' treatments of the theory of operation of the FPS, to describe specific instrument designs, and to outline practical procedures for using this instrument in both static and scanning modes. I have drawn freely from the results obtained by Connes, particularly those contained in Ref. 2. In those cases where our results differ, it is generally because I consider only relatively high reflection mirrors with uniform transmission, whereas Connes described interferometers in which the mirrors had zero transmission (and nearly complete reflection) over half of their apertures.

Following the introduction of curved mirror resonators as laser cavities, it was found that with little modification they could effectively be used as spectrum analyzers. Fork *et al.* have analyzed spherical mirror interferometers in general terms, and have demonstrated the extraordinarily high resolutions that can be obtained, particularly when the interferometer has optical gain as in a subthreshold laser.[6] While they recognized that confocal resonators (or spherical mirror Fabry-Perot interferometers—the two terms are interchangeable) offer certain distinct advantages over nonconfocal arrangements, the tendency to date has been to use nonconfocal cavities for high spectral resolution with laser light sources. The advantages of a nonconfocal arrangement are (a) the relatively loose tolerance on the mirror separation, and (b) the ability to select various free spectral ranges with a given pair of mirrors. Its disadvantages are (a) the necessity to match the input radiation field to a transverse mode of the cavity, and (b) the relatively low light gathering power of the resonator with spatially incoherent sources. The FPS, on the other hand, requires a relatively precise control of the mirror separation with a resulting fixed free spectral range. This disadvantage is largely offset by the high light gathering power of the FPS (even at very high resolution), freedom from mode matching considerations, and the capability of the instrument to be used to display spectral information in the form of a multiple beam interference fringe pattern. The FPS is clearly superior to a nonconfocal resonator for use with spatially incoherent sources and with fast pulsed light sources. It is also very much easier to use with cw laser sources and permits the spectral analysis of lasers operating in a number of different transverse modes.

Section II deals with the theory of the FPS and includes subsections on the localized fringe pattern, spectral resolution and instrument profile with finite apertures, light gathering power, and mode matching considerations.

Section III contains descriptions of prototype scanning and static FPS spectrum analyzers and practical procedures for their optimum use. We have been able to achieve finesses well in excess of 150 with both 5-cm and 10-cm mirror spacings: both instruments are thermally compensated and mechanically stable, and the 5-cm FPS incorporates a piezoelectric scanning device which permits its use in either a static or rapid scan mode.

Table I lists the symbols used.

The author is with the Institute of Optics, University of Rochester, Rochester, New York 14627.

Received 2 January 1968.

This work supported in part by the Air Force Cambridge Research Laboratories.

Table I. List of Symbols

A	=	area of FPS entrance aperture
c	=	velocity of light
d	=	FPP mirror separation
D	=	aperture diameter (FPS or FPP)
F	=	finesse = $(\pi R/(1-R^2)$, (FPS)
L	=	cavity loss per transit
M	=	fringe pattern magnification factor
r	=	FPS mirror radii and confocal separation
R	=	mirror reflectivity
$\mathfrak{R}$	=	spectral resolving power
T	=	mirror transmission
T_0	=	FPS instrumental transmission
U	=	étendue = ΩA
δ	=	phase increment = $2\pi\Delta/\lambda$
Δ	=	path difference
ϵ	=	difference between FPS mirror separation and confocal spacing r.
λ	=	wavelength
ν	=	optical frequency
$\Delta\nu_m$	=	minimum resolvable frequency difference, or instrumental bandpass.
$\Delta\nu_f$	=	free spectral range, $c/4r$(FPS)
ρ	=	fringe radius
ρ_s	=	radius of central spot = $(\lambda r^3/F)^{\frac{1}{2}}$
Ω	=	solid angle subtended by source

II. Theory of Operation

A. Interference Fringes

A spherical mirror Fabry-Perot interferometer is comprised of two identical spherical mirrors separated by a distance very nearly equal to their common radius of curvature. When light from a source lying close to the axis is incident on the FPS, a multiple beam interference pattern is produced in the vicinity of the central plane of the interferometer. To see how this interference pattern arises, consider an entering ray which intersects the two mirrors at points P_1 and P_2, which are located at distances ρ_1 and ρ_2 from the axis. As shown in Fig. 1, θ is the skew angle of the entering ray. According to paraxial optics, each mirror serves to image the other mirror back upon itself, so that a paraxial ray is reentrant, i.e., falls back upon itself, after traversing the interferometer four times [Fig. 2(a)]. Owing to aberration, however, a general ray is not reentrant but follows a path such as that shown in Fig. 2(b). Even though it is not reentrant, if the incident ray is not at too great an angle to the axis, it will continue to intersect itself in the vicinity of a point P, located in the central plane of the FPS at a distance ρ from the axis. The position of the points at which rays continue to intersect themselves determines the position of the fringe pattern. If the axial mirror spacing is precisely r, the mirror radius, it is straightforward to show that the four-transit path, i.e., the path taken between successive intersections at the point P, exceeds the paraxial path $4r$ by an amount:

$$\Delta_0 = \rho_1^2\rho_2^2 \cos 2\theta/r^3 + \text{higher order terms.} \quad (1)$$

More generally, if the mirror spacing is $(r+\epsilon)$, the four-transit ray path exceeds the corresponding paraxial ray path $4(r+\epsilon)$ by an amount:

$$\Delta = \rho_1^2\rho_2^2 \cos 2\theta/r^3 + 2\epsilon(\rho_1^2+\rho_2^2)/r + \text{higher order terms.} \quad (2)$$

If we now restrict our attention to a small and distant source, close to the axis of the interferometer, we may write for Eq. (2):

$$\Delta(\rho) \simeq \rho^4/r^3 + 4\epsilon\rho^2/r^2, \quad (3)$$

where ρ is the height at which an entering ray crosses the central plane of the FPS. Refering to Fig. 2(b) we see that for each entering ray there are two sets of transmitted rays: those which have been reflected $4m$ times (type 1), and those which have been reflected $(4m+2)$ times (type 2), where m is an integer. The interference

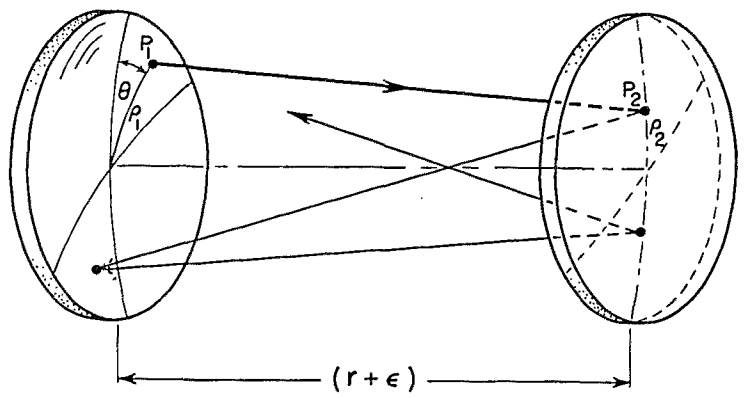

Fig. 1. General ray path in a spherical mirror Fabry-Perot interferometer.

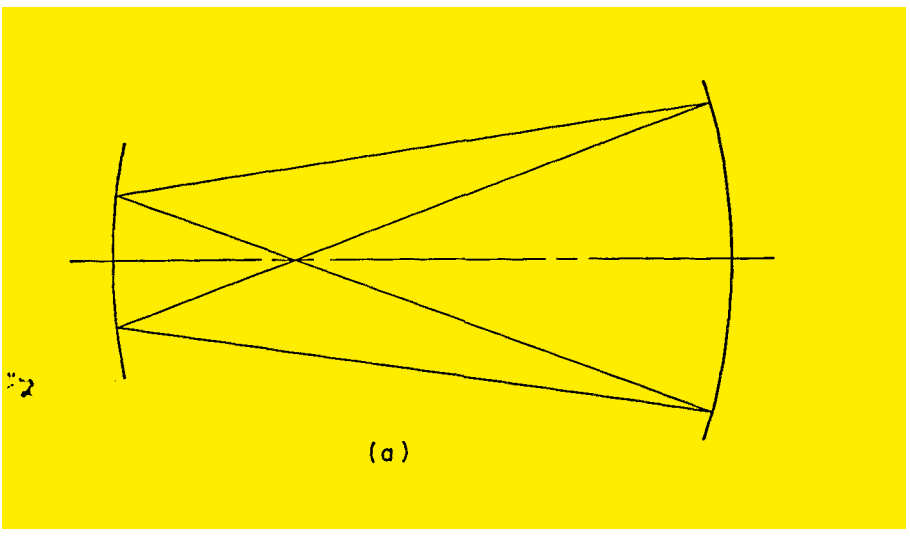

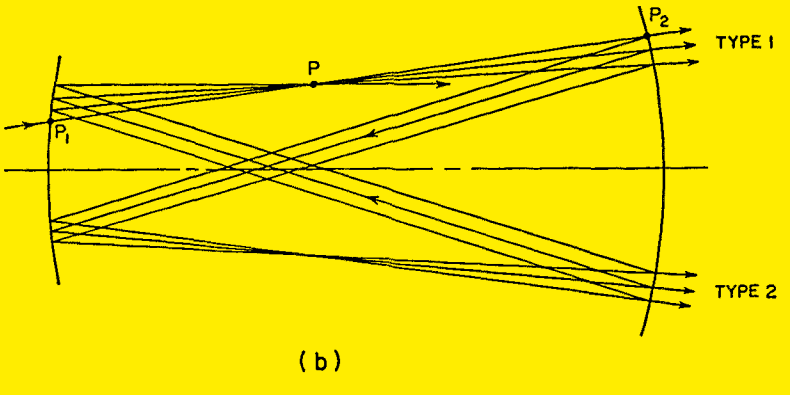

Fig. 2. (a) Ray path in an FPS in the paraxial approximation (reentrant rays), (b) aberrated ray path, showing intersection of rays at point P.

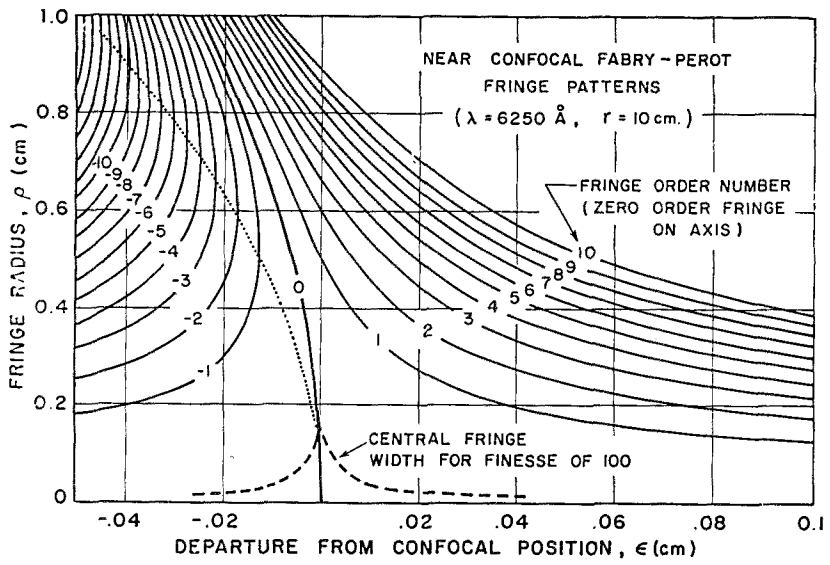

Fig. 3. Near confocal FPS fringe patterns. At each value of ϵ, the solid curves give the radii of the circular interference fringes for the case of a monochromatic source and a bright fringe on axis. The dashed line shows the spot size radius ρ_s for a finesse of 100, and the dotted line defines the zone of best focus as a function of ϵ. (Appendix I shows how to change the scales for different wavelengths and mirror separations.)

patterns produced in the central plane of the interferometer are described by:

Type 1:

$$I_1(\rho,\lambda) = I_0[T/(1-R^2)]^2\{1 + [2R/(1-R^2)]^2 \times \sin^2[\delta(\rho,\lambda)/2]\}^{-1} \quad (4a)$$

or,

Type 2:

$$I_2(\rho,\lambda) = R^2 I_1(\rho,\lambda) \quad (4b)$$

where,

$$\delta(\rho,\lambda) = (2\pi/\lambda)[\Delta(\rho) + 4(r+\epsilon)]. \quad (5)$$

(See Table I for a list of symbols.) The derivation of these equations exactly follows the usual derivation for a plane mirror Fabry-Perot interferometer (FPP). When the mirror reflectivity R is close to unity, the interference patterns for both types of rays are the same and are superposed. When the two types of ray leave the interferometer at a small angle, e.g., if the entering beam is approximately collimated but at an angle to the axis, they will form an additional interference pattern made up of equally spaced straight fringes whose separations are determined by the angle at which the two beams are brought to focus. This two-beam, i.e., $\sin^2$, interference pattern modulates the multiple beam pattern of circular fringes and, of course, arises only when the two beams are coherent. Examples of this incidental two-beam pattern are shown in Sec. III.

From Eq. (4) we see that bright fringes are formed in the central plane of the interferometer when $\delta(\rho,\lambda)$ satisfies $\delta(\rho,\lambda) = 2m\pi$, or,

$$\rho^4/r^3 + 4\epsilon\rho^2/r^2 = m\lambda, \quad (6)$$

where m is a positive or negative integer giving the order of interference relative to the order on axis (which is assumed, for convenience, to be an integer). Fringes thus have radii given by:

$$\rho_m = [-2\epsilon r \pm (4\epsilon^2 r^2 + m\lambda r^3)^{\frac{1}{2}}]^{\frac{1}{2}}. \quad (7)$$

For $\epsilon > 0$, ρ_m is single-valued and $m > 0$. When $\epsilon < 0$, ρ_m is two-valued for $m \leq 0$, and single-valued for $m > 0$. Figure 3 shows this fringe pattern in cross section for different values of ϵ with r and λ fixed. (Appendix I shows how to transform this curve, as well as curves in later figures, so that it corresponds to other values of r and/or λ.)

The maximum radial dispersion in the fringe pattern $(d\rho/d\lambda)$ is obtained in the vicinity of the fringe corresponding to the lowest order of interference. For any given value of ϵ this fringe occurs at the value of ρ which corresponds to the *zone of best focus* for the spherical mirror. (By Fermat's principle, this is just the value of ρ where $d\Delta/d\rho$ is an extremum, or $\rho = (-2\epsilon r)^{\frac{1}{2}}$. No zone of best focus is defined for $\epsilon > 0$.)

In the special case (very nearly approximated in most applications) where $\epsilon \approx 0$, the fringes have radii given by:

$$\rho_m = [(m-\xi)\lambda r^3]^{\frac{1}{4}}, \quad (8)$$

where $\xi < 1$ and $[4(r+\epsilon)/\lambda]$ is the exact order of interference on the axis.

It is obvious from Eq. (8) that the radial dispersion in the fringe pattern is markedly nonlinear near the axis when the interferometer is precisely confocal. This is, of course, no real disadvantage and provides the basis for the high étendue of which this type of instrument is capable. If desired, the dispersion may be made more nearly linear by slightly decreasing (or increasing) the mirror separation. This is evident from Fig. 3 and is illustrated in Sec. III.

B. Spectral Resolving Power

In discussing spectral resolving power in this section, we assume that the interferometer is set at the confocal spacing ($|\epsilon| \leq \lambda$) and is used in the scanning mode with a collimated light source. More specifically, we assume that the central fringe pattern is imaged, 1 to 1, onto a plane containing an axial aperture, coincident with the center of the fringe pattern, behind which is located a linear detector. Since the resonant wavelength of the interferometer is a linear function of the mirror spacing, it is possible to obtain a linear plot of the source spectrum simply by recording the output from the detector as a function of the mirror separation. A change of $\lambda/4$ in the mirror separation scans through a free spectral range of $c/[4(r+\epsilon)]$ Hz.

The spectral resolving power $\mathcal{R}$ of a spectroscopic instrument is defined by:

$$\mathcal{R} \equiv \nu/\Delta\nu_m = \lambda/\Delta\lambda_m, \quad (9)$$

where $\Delta\nu_m$ is the minimum resolvable frequency increment in the vicinity of a frequency ν. The classical criterion for defining what is meant by *minimum resolvable increment* is an extension of the criterion used by Rayleigh in discussing diffraction pat-

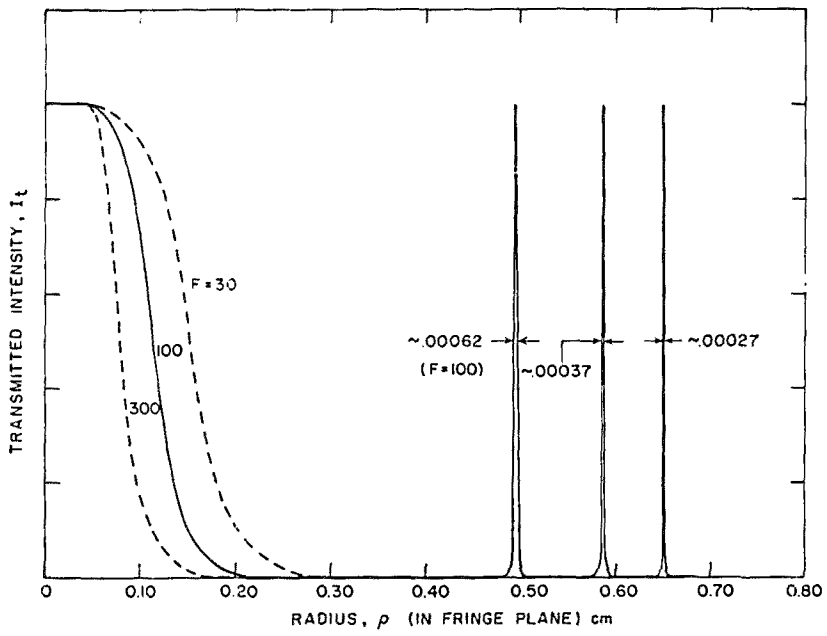

Fig. 4. Calculated distribution of light in an FPS fringe pattern for a monochromatic source and various values for F, the finesse. Note the broad central fringe ($\epsilon = 0$, $r = 10$ cm).

terns. For convenience, we depart from this definition slightly and define the *minimum resolvable frequency increment* as the apparent spectral width (full width at half maximum) of a monochromatic line. This is, of course, just the width of the instrumental profile. In practice, a large number of factors enter into the determination of the instrumental profile of a Fabry-Perot interferometer. These include mirror reflectivity, mirror figure, diffraction losses, and alignment. One of the great advantages of the spherical Fabry-Perot interferometer over its plane parallel counterpart is the relative ease with which reflectivity limited resolution can be realized in practice. Neglecting all but transmission losses at the mirrors, the instrumental profile of an FPS is given by Eq. (4). The resulting value for $\Delta\nu_m$, the width of the instrumental profile, is given by:

$$\Delta\nu_m = c(1 - R^2)/4\pi rR. \tag{10}$$

At this point it is useful to introduce a quantity called the finesse F of the interferometer, which we can define as the ratio of the free spectral range to the instrumental width:

$$F \equiv \Delta\nu_f/\Delta\nu_m. \tag{11}$$

In terms of the finesse F, the instrumental width and spectral resolving power are given by:

$$\Delta\nu_m = C/4rF, \tag{12}$$

and

$$\mathfrak{R} = 4rF/\lambda. \tag{13}$$

Also, the expression for the interference pattern can be written as:

$$I(\rho) = \left(\frac{T}{1 - R^2}\right) \frac{I_0}{1 + (2F/\pi)^2 \sin^2(\delta/2)}. \tag{14}$$

Here we have simply made the substitution, $F = \pi R/(1 - R^2)$ in Eq. (4). Note that this expression *remains* valid regardless of whether the finesse is determined by the mirror reflectivity, or by other factors. When the finesse is limited by a mirror reflectivity whose value is close to unity, we have:

$$F_R = \pi R/(1 - R^2) \approx \pi/2(1 - R). \tag{15}$$

The fringe pattern described by Eq. (14) is shown in Fig. 4 for representative values of the finesse.

In order to record the ultimate instrumental profile in the scanning mode of operation, the detector aperture would be vanishingly small and the resulting instrumental profile would be given by:

$$I(\nu - \nu_0) \simeq (\tfrac{1}{4})[T/(1 - R)]^2 I_0(\nu) \times \left\{1 + \left[\frac{2(\nu - \nu_0)F}{c/4r}\right]^2\right\}^{-1}. \tag{16}$$

If the detector aperture were increased, there would initially be an increase in the amount of light collected from a finite source, with little decrease in resolving power (assuming perfectly spherical mirrors and confocal spacing). As the aperture was opened further, the amount of light collected would increase less rapidly and the resolving power would begin to decrease—becoming approximately 70% of the resolving power given by Eq. (16) when the radius of the detector aperture attained a value ρ_s given by:

$$\rho_s = (r^3\lambda/F)^{\frac{1}{4}}. \tag{17}$$

We will refer to ρ_s as the *spot size* or *spot radius*; ρ_s is simply the radius of the mirror zone whose resonant frequency is displaced from the axial resonance by an

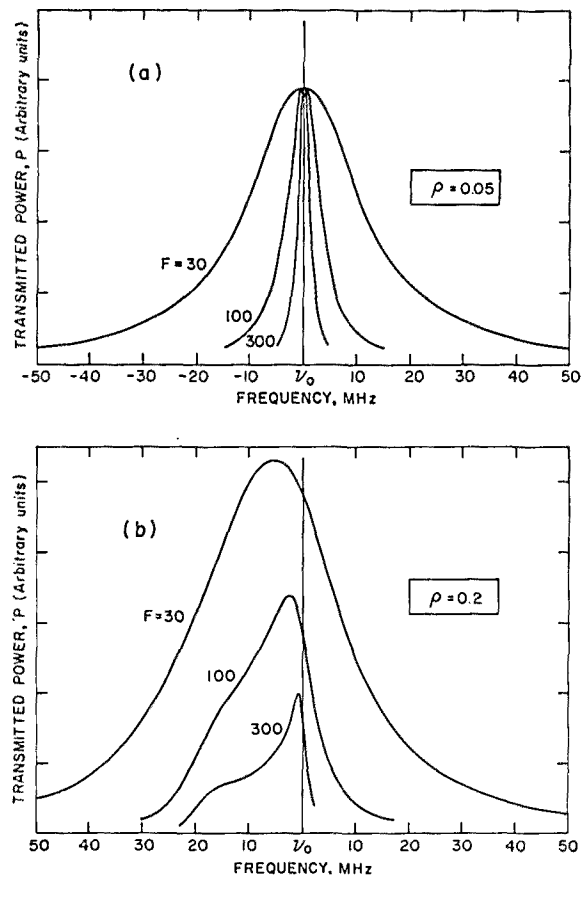

Fig. 5. Calculated FPS instrumental profiles for two different detector aperture radii. These correspond to the spectra which would be recorded using a monochromatic source in the scanning mode of operation ($\epsilon = 0$, $r = 10$ cm). (a) $\rho = 0.05$, (b) $\rho = 0.2$.

amount equal to the minimum resolvable frequency increment $\Delta\nu_m$. The actual instrumental profile that is obtained when using a finite detector aperture is given by:

$$I_p(\nu - \nu_0) = 2\pi \int_0^\rho I(\xi)x\,dx, \tag{18}$$

where

$$\xi = [\nu - \nu_0(1 + x^4/4r^4)]$$

and

$$I(\xi) = \tfrac{1}{4}\{(T/(1 - R)^2 I_0\{1 + (2F/\pi)^2 \sin^{-2}[\pi\xi/(c/4r)]\}^{-1},$$

and where ν_0 is the frequency that would be recorded using a vanishingly small aperture. Note that with a finite aperture, the instrumental profile is no longer centered on ν_0 and is asymetric. Figure 5 shows computed instrumental profiles for various values of F and ρ, the aperture radius (cf., Fig. 14 in Sec. III).

Other Factors Affecting Instrumental Finesse

We have seen [Eq. (15)] that in the absence of other losses, the instrumental finesse is limited by the reflectivity of the mirrors to a value of approximately $\pi/[2(1 - R)]$. In this section we consider the manner in which the finesse is degraded by other factors, namely, irregularities in the surfaces of the mirrors, and diffraction. If we wish, we can associate with each loss mechanism, e.g., mirror transmission or diffraction, a contribution to the lifetime of the resonant cavity. The finesse F_i associated with the ith loss mechanism, is related to the corresponding contribution to the cavity lifetime τ_i by:

$$F_i = \pi c\tau_i/2r. \tag{19}$$

Hence it is clear that the net instrumental finesse F is related to the individual contributions F_i by:

$$F^{-1} = \sum_i (F_i)^{-1}, \tag{20}$$

so that it is useful and meaningful to consider the individual contributions to the finesse independently.

First we consider the effect of irregularities in the figure of the mirror on the finesse. Without knowledge of the specific nature of these irregularities, it is impossible to be precise in predicting their effect on the finesse. Generally, however, if the mirrors have a *smooth** irregularity on the order of λ/m across the aperture being used, then the figure-limited finesse F_f will be approximately:

$$F_f \approx m/2. \tag{21}$$

Obviously, by reducing the aperture (or diameter of the incident light beam) it is possible to minimize the reduction in instrumental finesse due to plate irregularities. This is indeed a practical expedient in the case of a spherical Fabry-Perot etalon; in the case of a plane mirror Fabry-Perot etalon, however, the significantly increased diffraction losses that accompany the reduction of the etalon aperture set a limit to the improvement in finesse that can be realized by this technique. Note also that in the case of the plane mirror Fabry-Perot, an angular misalignment of the plates is equivalent to a corresponding plate imperfection. For the spherical Fabry-Perot, this is not the case: an angular misalignment merely redefines the optical axis of the system. With regard to plate irregularities, it is worthwhile pointing out another contrast between the plate-mirror and spherical-mirror etalons. If the mirrors of an FPP have irregularities on the order of $\lambda/2$, the resultant pattern at infinity will be completely washed out. However, since the fringe pattern obtained with an FPS is localized relatively close to the surfaces of the mirrors, a similar mirror figure irregularity will *not* wash out the fringe pattern, but will instead distort it so that the fringes are no longer circular. (These distorted fringes tend to define coutours of equal path difference.)

As implied above, diffraction losses are much less in the case of a spherical Fabry-Perot etalon than for its plane mirror counterpart. The rigorous justification of this statement lies in the analytical treatment of confocal resonators given by Boyd and Gordon,[7] in which they show that for any case of practical interest to us, i.e., those cases where $D^2/4r \gg \lambda$, D being the diameter of the mirror aperture, the diffraction losses for a confocal resonator are orders of magnitude less than for the corresponding plane parallel resonator. The calculation of the exact diffraction loss in a confocal resonator requires a fairly complex analysis in which the incoming radiation field is decomposed into eigenmodes of the cavity, each of which has a different diffraction loss. Absolute minimization of the diffraction losses requires proper mode matching (see Sec. II.D). In this case, when the incoming radiation field has a curvature and amplitude distribution identical to that of the lowest order transverse mode of the confocal resonator, the diffraction loss per pass L_D is approximately given by[7]:

$$L_D \approx 10^{-[5(\rho_0^2/r\lambda)+1]} \tag{22}$$

where ρ_0 is the radius of the mirror aperture. In any case of practical interest, diffraction losses are completely negligible in comparison to other losses, so that diffraction plays no significant role in determining the over-all finesse. For a plane parallel Fabry-Perot etalon, the diffraction limited finesse is approximately given by:

$$F_D(\text{FPP}) \simeq D^2/2\lambda d, \tag{23}$$

where d is the separation of the plane mirrors and D is the aperture diameter.

Other types of loss, such as scattering at the mirror surface (which is, of course, taken into account in F_R), can be treated separately very easily. If a small fraction L of the radiation incident on the mirror (or making a transit of the resonator) is lost, then by analogy to

* If the irregularity is not smooth, the loss incurred is more appropriately treated as a scattering loss.

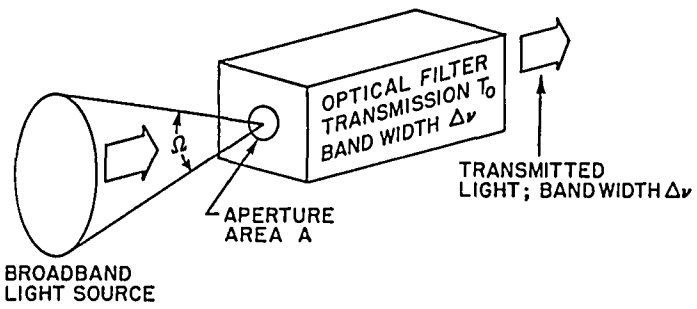

Fig. 6. Generalized picture of a spectrometer or monochrometer.

Eq. (15), the corresponding contribution to the finesse is given by:

$$F_L \sim \pi/2L. \tag{24}$$

To summarize the implications of this section, we can say that for a spherical Fabry-Perot interferometer, in confocal adjustment, the significant factors in determining the finesse and resolving power are the reflectivity of the mirrors and their surface figure. This is in contrast to the case of a plane parallel Fabry-Perot, where diffraction and alignment can make significant contributions to the degradation of finesse and resolving power.

C. Light Gathering Power

1. *Introduction*

One of the major factors to consider in evaluating any spectrometer is its ability to effectively gather light from an incoherent extended source, filter it with the instrumental bandpass, and transmit it to some radiation detector. In general, the situation can be represented by Fig. 6. Here, the spectrometer is depicted as a bandpass filter: all of the radiation emanating from within a solid angle Ω subtended at an aperture of area A, can be transmitted within the bandpass $\Delta\nu_m$ of the spectrometer. If the transmission of the spectrometer at the center of the bandpass is T_0 and the spectral radiance of the source is N_ν, then the radiant power per unit bandwidth P_ν transmitted by the spectrometer is given by:

$$P_\nu = N_\nu A\Omega T_0. \tag{25}$$

The product ΩA has come to be known as étendue U of the spectrometer. Thus the easily remembered expression:

$$P = NUT_0. \tag{26}$$

Of course, if the light source under investigation is a laser, it is obvious that most of the emitted power can be put into a beam with a small cross-sectional area and a small divergence. In this case, the étendue of the spectrometer provides a measure of the *alignment tolerance* between the laser beam and spectrometer, rather than being a measure of the spectrometer's light gathering power.

2. *Transmission and Étendue of a Spherical Fabry-Perot Interferometer*

In Sec. II.A it was pointed out that a single beam of light incident on an FPS gives rise to two transmitted beams, which are generally at a small angle to one another. When both of these transmitted beams are taken into account, the net transmission T_0 at the center of the instrument profile is found from Eq. (4a) and (4b):

$$T_0 = (1 + R^2)(T/[1 - R^2])^2 \approx \tfrac{1}{2}[T/(1 - R)]^2, \text{ for } R \approx 1. \tag{27}$$

(When the two transmitted beams are precisely aligned, the situation is somewhat different, as discussed in Sec. II.D.) If we define A to be the sum of the absorption and scattering at the mirrors, then $(1 - R) = (T + A)$, so that the peak transmission may be written as:

$$T_0 \approx \tfrac{1}{2}[1 + (A/T)]^{-2} \tag{28}$$

This function is plotted in Fig. 7, which clearly illustrates the drastic loss in net transmission whenever the absorption-plus-scattering losses become comparable with, or exceed, the transmission loss at the mirror. As a rule, very high reflectivities can be attained only at the expense of increased values of (A/T), so that it is often necessary in practice to make a compromise between finesse and transmission. This type of compromise is discussed further in Sec. III.

In the last section we found that the ultimate instrumental resolution, which we now call $\mathcal{R}_0$, could be obtained only with an infinitesimally small axial aperture. In this case, of course, the étendue is also infinitesimal. A reasonable compromise between spectral resolving power and étendue can be reached by increasing the mirror aperture until the resolving power $\mathcal{R}$ is reduced to a value of approximately 0.7 $\mathcal{R}_0$. This, as we have seen, occurs when the mirror apertures have radii of approximately ρ_s. Under this condition, the étendue is given by:

$$U = [\pi\rho_s^2][\pi\rho_s^2/r^2] = \pi^2 r\lambda/F, \tag{29}$$

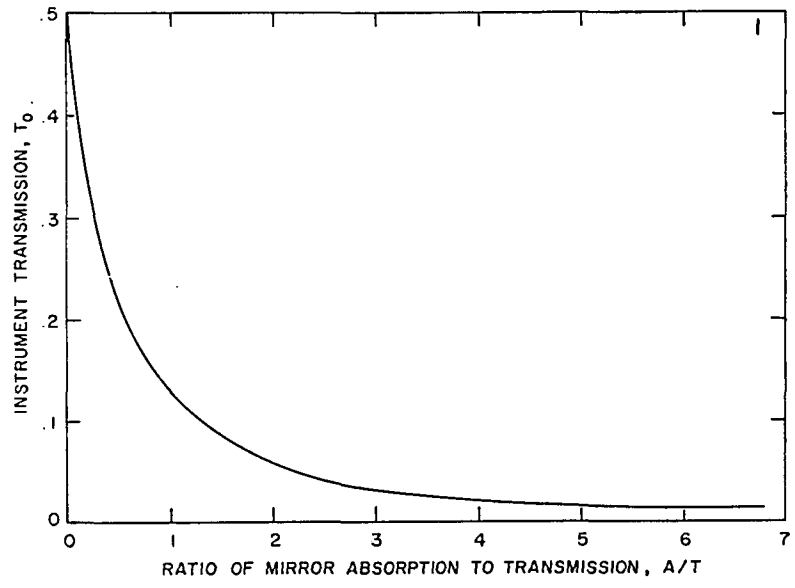

Fig. 7. FPS instrumental transmission as a function of the (absorption:transmission) ratio of the mirror coatings.

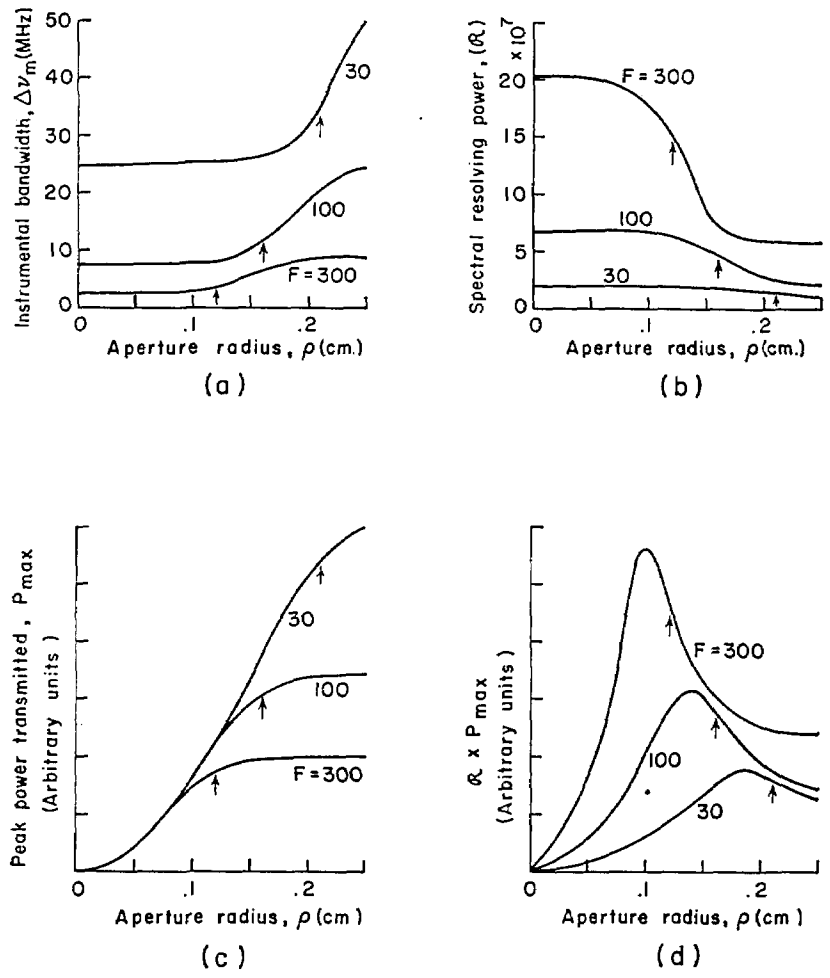

Fig. 8. Computed FPS characteristics as a function of detector aperture radius ρ for different values of F, the finesse. Arrows indicate the value of ρ_s in each case ($\epsilon = 0$, $r = 10$ cm). The maxima in the curves shown in (d) define the aperture radius giving the best compromise between resolving power and peak transmitted power.

where F is the finesse which determines the value of ρ_s according to Eq. (17).

Figure 8 shows computed curves for the instrumental bandwidth, spectral resolving power, peak transmitted power, and the product (peak transmitted power) $\times$ (resolving power), all plotted as a function of aperture radius for finesses of 30, 100, and 300. These curves show that the resolution drops to about $0.7R_0$ when the aperture is opened up to a value of $\rho_s \equiv (\lambda r^3/F)^{\frac{1}{2}}$. Figure (8d), however, shows that the value of ρ which maximizes the product of the spectral resolving power and power transmitted is approximately $0.8\rho_s$. In practice, the most convenient way to quickly attain a useful compromise between resolution and transmitted power is to start with a relatively large aperture and, while observing the scanned spectrum of a narrow band source, to reduce the aperture size until the transmitted power at the peak of a displayed spectral line is reduced by between 20% and 30%. For this technique to be useful, of course, the mirror spacing must be very nearly confocal. This can be accomplished without much difficulty, as described in Sec. III.

3. *Comparison of FPS and FPP*

As Connes has pointed out, it is a unique characteristic of the FPS, amongst all other types of spectrometers, that, as the resolving power at constant finesse is increased (by increasing the mirror radii and separation), so also is the étendue.[1] In fact, the quotient $\mathcal{R}/U$ is a constant:

$$(\mathcal{R}/U)_{FPS} \approx 0.7(2F/\pi\lambda)^2. \tag{30}$$

In writing this expression, we accept the 20% to 30% loss in resolution which accompanies the realization of the étendue U. We also assume that, as the mirror radius is increased to realize higher resolving powers, we are able to maintain the required figure of $\approx\lambda/F$ across the central part of the mirror having a radius ρ_s. It is interesting to compare this behavior with that of an FPP. We assume that for an FPP, a net surface figure (including alignment error) of λ/F can be maintained across plates of diameter D, which are separated by a distance d. For this FPP the étendue is $(\pi D^2\lambda/4dF)$, and the resolving power is $(2df/\lambda)$, so that it is the *product* of the resolving power and étendue which remains constant:

$$(U\mathcal{R})_{FPP} \approx 0.7(\pi D^2/2). \tag{31}$$

(The factor of 0.7 again represents the loss in resolving power associated with a useful étendue.) Thus an increase in light gathering power must be paid for by a loss in resolution, and vice versa. The corresponding product for an FPS is given by:

$$(U\mathcal{R})_{FPS} \approx 0.7(4\pi^2r^2). \tag{32}$$

From this expression we see that by increasing the mirror radius of an FPS the étendue resolution product may be increased indefinitely as long as the mirror figure can be maintained to within λ/F across an aperture of diameter $2\rho_s \equiv 2(\lambda r^3/F)^{\frac{1}{2}}$.

At this point, it should be quite clear that at high resolution, and correspondingly small free spectral range, the FPS excells over the FPP, both in terms of étendue and resolution. As the free spectral range is increased, however, there will be some point at which the FPP will become the better choice in terms of étendue. The specific value of r, the mirror spacing of the FPS, at which this transition occurs depends upon both the desired finesse and the accuracy with which the mirrors of the FPP can be figured and aligned. If we define an angle α to represent the figure-plus-alignment accuracy required to maintain a finesse F, with a plate diameter D:

$$\alpha = (\lambda/FD), \tag{33}$$

then the ratio U_{FPS}/U_{FPP} may be written:

$$U_{FPS}/U_{FPP} = 4rdF^2\alpha^2/\lambda^2, \tag{34}$$

where d is the plate separation of the FPP and where we tacitly assume that the spot size ρ_s on the FPS is small enough so that there is no problem in maintaining the necessary figure of λ/F. If we now require that both the FPP and FPS have the same free spectral range, so that $d = 2r$, then Eq. (34) can be used to find the value of r at which the FPP becomes the better choice with regard to étendue:

$$r^* = (\lambda/\alpha)/2F. \tag{35}$$

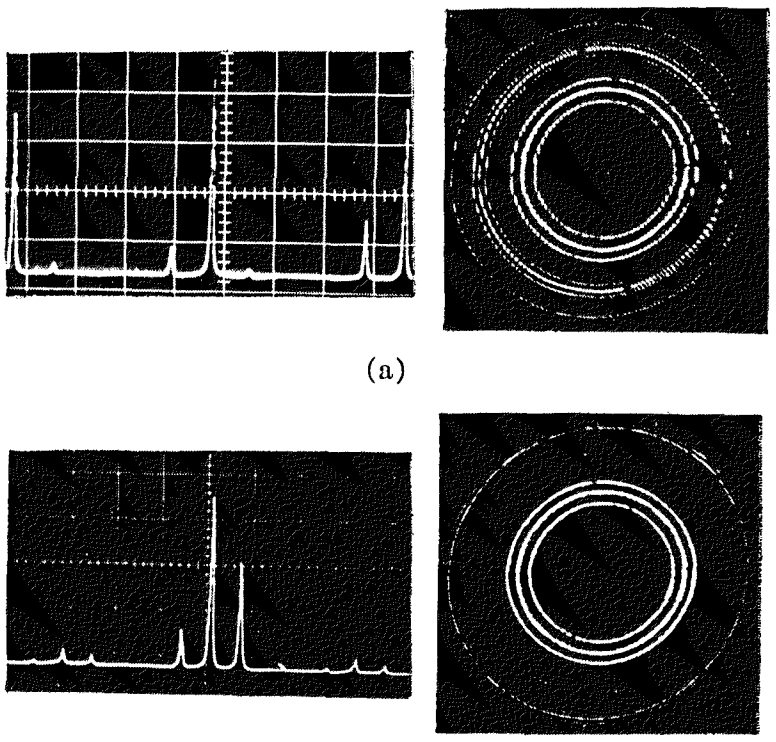

Fig. 9. (a) Scan and fringe displays of an FPS in normal operation. Note the secondary fringe pattern. (b) Scan and fringe displays of a very nearly mode-matched FPS. The alignment of the FPS relative to the source has been adjusted to eliminate the secondary fringe pattern, resulting in a doubling of both the free spectral range and the instrumental transmission. ($\epsilon \sim 20\ \mu$, $r = 5$ cm; three-mode laser source.)

For example, if the mirrors of an FPP can be maintained plane and parallel to within a hundredth of a wavelength per cm of aperture, so that (λ/α) is 100, and a finesse of 25 is desired, then an FPP offers the greater étendue up to a mirror spacing of 4 cm. Rather than increasing the FPP mirror spacing beyond 4 cm, one should in principle, switch to an FPS in order to obtain higher resolution and maximum étendue.

D. Mode Analysis of an FPS

The equations derived earlier in this section have been based primarily on a geometrical analysis of a confocal resonator, or FPS. This, as it turns out, is adequate for most purposes. A more rigorous treatment, however, would involve a decomposition of the incident radiation field into eigenmodes of the resonator, as defined (in the curved mirror case) by Boyd and Gordon.[7] In this section we outline an analysis of this sort and to some extent justify the simpler geometrical approach. We should point out that the *aberrations* of a confocal spherical mirror resonator, which give rise to the multiple beam interference fringes described earlier, can be conveniently analyzed only by the geometrical approach.

As shown by Boyd and Gordon, the eigenmodes TEM_{mnq} of a confocal resonator are closely approximated by Gaussian-Hermite functions [Ref. 7, Eq. (20)]. The first two subscripts m and n denote the amplitude distribution of the eigenmode on a surface of constant phase, and the third subscript q is the so-called axial mode number giving the number of axial modes in the intracavity standing wave. For the general case of a resonator made up of two mirrors, radii b_1 and b_2, separated by a distance d, Boyd and Kogelnik have shown that the resonant frequency associated with a given TEM_{mnq} mode is given by:

$$\nu_{mnq} = (c/2d)\{q + (1/\pi)(1 + m + n) \times \cos^{-1}[(1 - d/b_1)(1 - d/b_2)]^{\frac{1}{2}}\}. \quad (36)$$

We interpret this as follows: an arbitrary quasi-monochromatic field, of frequency ν_0, which is incident on a curved mirror resonator, is decomposed into a large number of transverse modes TEM_{mn}. Each of these transverse modes will be resonant, i.e., will be transmitted by the high Q cavity, for mirror separations satisfying:

$$d = (c/2\nu_0)\{q + (1 + m + n) \times \cos^{-1}[(1 - d/b_1)(1 - d/b_2)]^{\frac{1}{2}}\}. \quad (37)$$

In general, therefore, a given quasi-monochromatic field will be decomposed into a large number of transverse modes, each of which is resonant for a different mirror separation. In order for a general curved mirror cavity to be useful as a scanning spectrum analyzer (or static filter), the input field must be reduced to a single transverse mode of the cavity, i.e., mode matched, so that the transmission of the cavity, as a function of mirror separation, can be unambiguously interpreted in terms of the frequency content of the input field. This can be accomplished without considerable loss of light only in the case of a laser light source operating in a single transverse mode.

For the special case of a confocal, or near confocal resonator, such as an FPS, Eqs. (36) and (37) become:

$$\nu_{mnq} \simeq [c/4(r + \epsilon)]\,[2q + (1 + m + n)], \quad (36a)$$

and

$$(r + \epsilon) \approx (c/4\nu_0)[2q + (1 + m + n)], \quad (37b)$$

where the mirrors have radii r and are separated by $(r + \epsilon) \approx r$. Thus, *all* transverse modes will resonate at cavity lengths of either,

$$(r + \epsilon) = (c/4\nu_0)(2l + 1);\ l \text{ an integer, } (m + n) \text{ even}, \quad (38a)$$

or

$$(r + \epsilon) = (c/4\nu_0)(2l);\ (m + n) \text{ odd}. \quad (38b)$$

If we assume that an arbitrary input field of frequency ν_0 is made up of an approximately equal number of even and odd transverse modes (a good approximation in any instance where mode-matching is not intentionally accomplished), then the cavity will be resonant for:

$$(r + \epsilon) = cl/4\nu_0;\ l \text{ an integer}, \quad (39)$$

and the multimode free spectral range will be

$$\Delta\nu_f(\text{multimode}) \simeq c/4r \quad (40)$$

If, on the other hand, the input field exactly matches a single mode of the cavity, the free spectral range is

$$\Delta\nu_f(\text{single transverse mode}) \simeq c/2r. \tag{41}$$

The transition from multimode to single mode excitation can be observed without undue difficulty, as illustrated in Fig. 9. (Note that the free spectral range increases by a factor of two for both scanning and static fringe modes of use of the FPS.) The tolerance on the alignment of the light beam relative to the axis of the FPS that is required for mode matched operation is on the order of λ/ρ_s, so that it is highly unlikely that this situation would be encountered inadvertently.

Mode matching of an FPS can also be considered from a more direct point of view. We have already mentioned the additional interference pattern arising from an angular misalignment of the two types of rays transmitted by the FPS. It is easy to show that, when these two types of transmitted beams are aligned, they are in phase on axis (assuming $r = m\lambda/2$), just out of phase at the first fringe off axis, in phase again for the second fringe, and so on. Thus the superposition of the two transmitted beams results in constructive interference in every other free spectral range, and destructive interference in the remaining orders—thereby effectively doubling the free spectral range and at the same time doubling the amount of light transmitted at a given resonance (when *constructive* interference occurs for the *transmitted* beams, *destructive* interference occurs for the two *reflected* beams).

The great advantage of the confocal FPS over a general curved mirror resonator is the freedom from the necessity to mode-match in order to observe a clean spectrum. This, as we have just seen, is due to the frequency degeneracy of even and odd transverse modes of a confocal cavity. It can readily be shown from Eq. (36) that the maximum value of $|\epsilon|$, the departure from exact confocal mirror spacing, which can be tolerated without allowing the TEM_{mn} transverse mode to resonate at an observably different mirror spacing from that at which the TEM_{00} mode is resonant, is given by:

$$|\epsilon|_{\max} = \pi r/2(1 + m + n)F \tag{42}$$

Thus an FPS with $r = 10$ cm and a finesse of 100 will begin to suffer a loss in effective finesse for $(m + n) \approx 100$ when $|\epsilon|$ becomes greater than about 15 μ. Thus the variation in the mirror separation which occurs during direct scanning (less than a wavelength) is too small to affect the transverse mode degeneracy. Of course if pressure scanning is employed, it is the wavelength of the light which is changed, not the mirror separation.

III. Experimental Work with the FPS

This section is concerned with the practical aspects of the FPS, including its design and fabrication, alignment procedures, and various modes of operation. A number of applications are illustrated in the latter parts of this section.

A. General Design Considerations

There are three separate aspects of the design problem: (1) the mechanical design; (2) the attainment of high finesse, and (3) the optical layout. Each of these is briefly discussed in the following paragraphs.

1. Mechanical Design

The key mechanical requirements are that the two mirrors be accurately and rigidly fixed relative to each other; that there be a provision for making fine adjustments to the mirror separation (either during or after fabrication); that the optical separation of the mirrors be insensitive to temperature and/or pressure variation; and that the interferometer assembly be mechanically isolated from vibration and acoustic pickup. The requirements for rigidity and freedom from vibration dictate that the mirrors be held in a common structure, rather than mounted, for example, on a lens bench. This, in turn, means that any transducer used for varying the mechanical separation of the mirrors must be an integral part of the interferometer. Mechanical isolation of the rigid interferometer assembly is readily accomplished by mounting it in an outer case using a soft suspension (in the specific designs described later in this section, the outer case could be sharply struck without producing a detectable change in the observed spectrum—indicating a stability in the length of the optical cavity on the order of a one hundredth of a wavelength or better).

Insensitivity to pressure variations can be accomplished only by sealing the container holding the interferometer. This must be done, in any event, if the interferometer is to be pressure scanned. Insensitivity to temperature variations can be achieved both by conventional compensation, in which the expansions of dissimilar materials compensate for one another, and by the use of very low expansion materials. In an interferometer intended to serve as a passive frequency standard, we have combined both methods. As long as this interferometer is at a uniform temperature, its length can be maintained to within one part in 10^8 over a range of a few degrees centigrade.

The fine adjustment of mirror separation can easily be obtained using a well-made threaded mount for one mirror cell. For example, we found that a 12.7-mm diam cell with 16 threads/cm could be manually adjusted with a precision of at least a tenth of a wavelength providing that the mirror separation could be monitored by observing the spectrum from a stable gas laser. (Most gas lasers are far less stable, both mechanically and thermally, than the interferometers described here.) We were pleasantly surprised to find that the same precision of motion could also be obtained with a relatively loose screw fit when the slop was taken up with a thin Teflon tape commercially available as a pipe dope.

2. Attainment of High Finesse

The attainment of high finesse requires that the mirrors be of excellent optical quality and that they be

Table II. Characteristics of Some Multilayer Reflective Coatings

Type	Region of high reflectivity	F	T_0	R
A	6200 Å to 7000 Å	225	0.45	0.993
B	4800 Å to 6900 Å	150	0.35	0.99
C	4900 Å to 6800 Å	180–200	0.02	0.992

coated with high reflectivity multilayer dielectric films. For scanning applications, only the central spot, of radius ρ_s, need satisfy these requirements. If the interferometer is used to observe fringes, however, the mirror figure should be good over a somewhat larger area to ensure that the fringes will be circular. Mirror blanks should be tested against the same master; they generally require final polishing by hand if they are to have the necessary figure—that is to say, if they are to be spherical to within λ/F, where F is the desired finesse. Final evaluation of the mirror figure can only be made after the mirror has been coated and tested as an interferometer component. Not only must the mirror figure be excellent, but the polished surface must be free of microscopic scattering sites if the ultimate in reflectivity is to be realized. This is within the present state of the art, and scattering losses of less than 0.3% are attainable with fused quartz blanks.*

As we suggested in the last section, one is usually forced to make some sort of compromise between finesse, instrumental transmission, and possibly the spectral bandwidth within which the mirrors have high reflectivity. For example, using commercially available multilayer coatings (referred to as types A, B, and C) we were able to obtain the performance summarized in Table II. Type A is a narrow band coating covering a rather restricted spectral range, but offers high finesse combined with excellent transmission. Type B covers a considerably broader portion of the spectrum with fairly high instrumental transmission, but has a somewhat reduced finesse. Type C, on the other hand, has broad band coverage and relatively high finesse, but rather low transmission. By making fairly drastic sacrifices in instrumental transmission, it is probably possible to obtain finesses of up to 500 with commercially available coatings and a passive interferometer. This limitation is not set by available reflectivity, but by attainable mirror figure (or diffraction losses in the case of very short cavities).

3. *Optical Layout*

By *optical layout* we mean the optical system which brings the light into the interferometer and determines the path of light leaving the interferometer. For a number of reasons we have preferred to make the interferometer mirror blanks of very nearly zero optical power. This permits the use of mirrors with concentric surfaces, which simplifies fabrication. More importantly though, it means that the interferometer can be used to spectrally filter a narrow collimated beam of light without appreciably affecting the collimation of the beam. If a further optical system is added to the FPS, it should serve to facilitate the alignment of the FPS with the light source, and to get light efficiently through the interferometer and within the instrumental passband. Figure 10 illustrates an optical system which has proved to be convenient and versatile. Consider first an incident collimated beam: lens L_1 brings the incident radiation to focus at the center of the interferometer. (Note that the path of light within the interferometer is just the reverse of the case where the light incident on the interferometer is collimated.) All of the light falling within a central circle of radius $2\rho_s f/r$ on lens L_1 will pass through the detector aperture of radius ρ_s and will thus be filtered by the instrumental passband. In this mode of operation the FPS can be used as a static or tunable filter, or as a scanning spectrum analyzer. If the incident light is not collimated, there is no significant loss in resolution, but there may be a reduction in the amount of light received by the detector. This holds even for gross departures from collimation in the incident beam of light. The entire system should be free to rotate about the center of L_1. In this way the incoming beam can be directed at the center of L_1 and then the entire interferometer system can be rotated about this point in order to attain alignment between the incoming beam of light and the axis of the FPS. The detector aperture, which limits the actual instrumental bandpass for incident beams with a large diameter, is located just behind the interferometer.

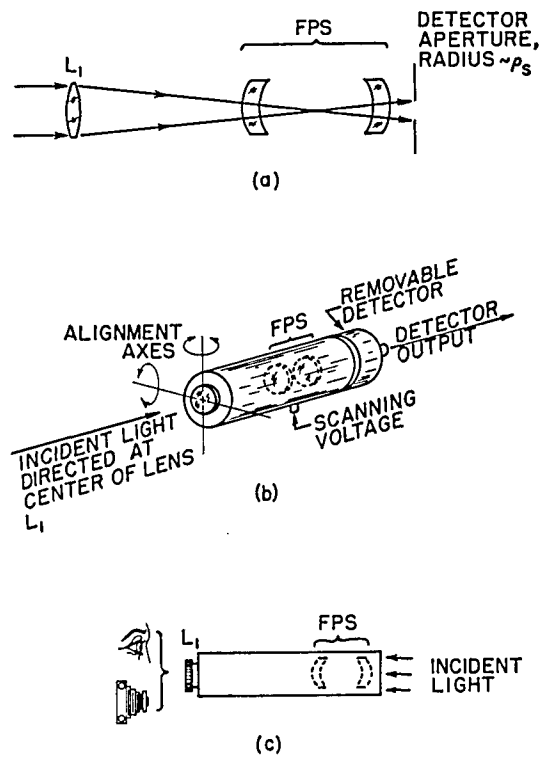

Fig. 10. A versatile FPS instrument. (a) Optical layout showing the FPS etalon, lens L_1, and detector aperture; (b) arrangement for scanning; (c) arrangement for observing and recording fringe pattern (detector removed).

* It is now generally recognized that essentially scatter-free surfaces of excellent figure can be obtained by *continuous* and *extended* (12–36 h) final polishing of fused quartz blanks.

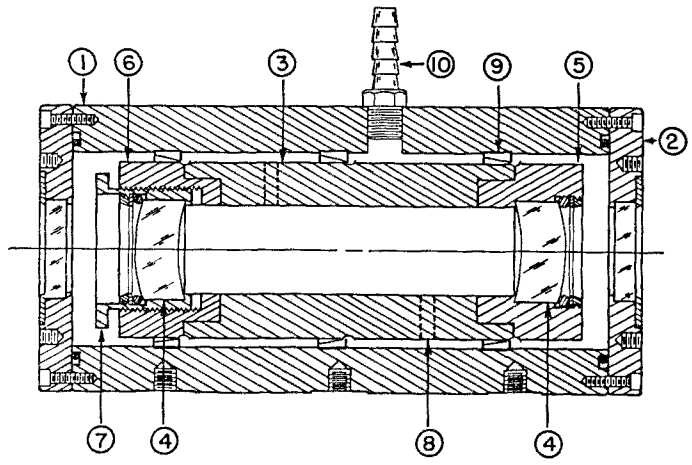

Fig. 11. Schematic of a highly stable fixed mirror FPS etalon: (1) outer case (Al alloy); (2) end plates with windows; (3) Cer-Vit etalon spacer; (4) fused quartz mirrors; (5) fixed mirror cell (Invar); (6), (7) adjustable mirror cell (Invar); (8) ports in etalon spacer; (9) phosphor bronze springs holding etalon; (10) fixture for evacuating chamber and pressure scanning.

This design facilitates the observation of the static fringe pattern. If the detector aperture is removed and a quasi-collimated beam of light is incident on what was the rear of the system, then the fringe pattern will be formed in the focal plane of lens L_1. Thus an observer, or camera focused on infinity, can readily view the fringe pattern. If the incident beam is diverging, rather than collimated, then the plane of the fringe pattern will be slightly displaced *towards* the lens, and vice versa. A low power focusing telescope is useful both for observing the fringe pattern, and for photographing it. In this mode of operation, the system should be mounted so that it can be rotated about a point near the right-hand interferometer mirror [Fig. 10(c)]. To use the interferometer as a narrow bandpass filter with zero optical power, the lens is simply removed.

In order to eliminate ghost fringe patterns, the rear surfaces of the FPS mirrors, and both surfaces of L_1, should be antireflection coated.

B. Design of a Static or Pressure Scanned FPS

This design, shown in Fig. 11, is intended primarily to eliminate variation of the axial mirror separation with temperature. This FPS is thus well suited for use as a secondary frequency standard with a long term stability of better than 1 MHz with temperature control of $\pm 1°$ C. This thermal stability is obtained by making the mirror spacer of Cer-Vit* (thermal expansion coefficient no greater than $\pm 0.1 \times 10^{-7}/°C$), and using the Invar mirror cells thermally to compensate for the residual expansion of the Cer-Vit (this can easily be done since the manufacturers of Cer-Vit routinely supply accurate expansion data for each blank). The quartz mirrors change radius by about a wavelength for a 1° C temperature change, but this introduces a negligible change in the mirror separation, which determines the resonant frequency of the FPS. We have not yet established the lower limit on the frequency stability of this system.

The interferometer assembly is held inside a pressure chamber by means of phosphor-bronze finger-stock springs, which provide adequate mechanical isolation. The pressure chamber can be used for pressure scanning, or it can be partially evacuated and sealed to eliminate effects due to changes in atmospheric pressure.

Applications for this type of interferometer include ultrahigh resolution spectroscopy, and use as a passive feedback component in frequency stabilizing lasers.

C. A Piezo-electrically Scanned FPS System

This instrument is designed along the lines illustrated in Fig. 10, and can be used as a scanning spectrum analyzer, as a tunable narrow bandpass filter with zero optical power, or for direct observation of multiple beam interference fringes. The key element in the instrument is the FPS etalon, which is comprised of a fixed and an adjustable mirror cell, and a thermally compensated rigid spacer tube. The spacer tube includes, as an integral component, a piezo-electric ceramic section which increases in length by about 1.5 cm $\times 10^{-5}$ cm with the application of 50 V across the inner and outer surfaces of the tube (sufficient to scan a complete free spectral range in the visible). The adjustable mirror cell permits the mirror spacing to be easily set to within a fraction of a micron. Further fine adjustment can be accomplished by applying a dc voltage to the scanning voltage terminal; this is the method of tuning in the bandpass-filter mode of operation. Figure 12 shows a cut-away view of the entire instrument.

The FPS etalon is mechanically isolated from the case by a mounting technique using two large silicone rubber O-rings which cushion the etalon from mechanical shocks (see Fig. 12). The outer case can be struck sharply from any direction without noticeably affecting the resonant frequency of the etalon. As shown in Fig.

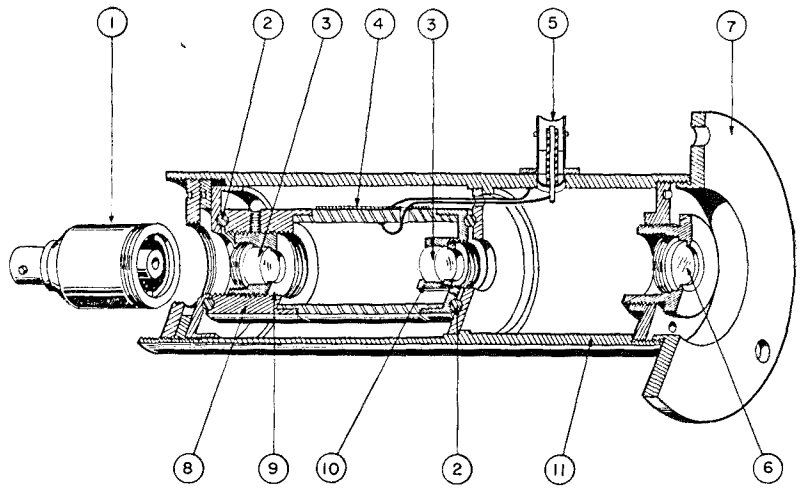

Fig. 12. An FPS spectrum analyzer for scanning or static mode of operation: (1) removable detector (photodiode); (2) soft O-ring for mounting FPS etalon; (3) quartz mirrors (r = 5 cm); (4) piezo-electric transducer/etalon spacer; (5) scanning voltage terminal; (6) auxiliary lens (focal point is between mirrors); (7) mounting flange; (8), (9) adjustable mirror cell; (10) fixed mirror cell; (11) outer case. (The mirror cells are designed to compensate for the thermal expansion of the etalon spacer.)

* Cer Vit is a low expansion semitransparent glasslike ceramic manufactured by Owens-Illinois.

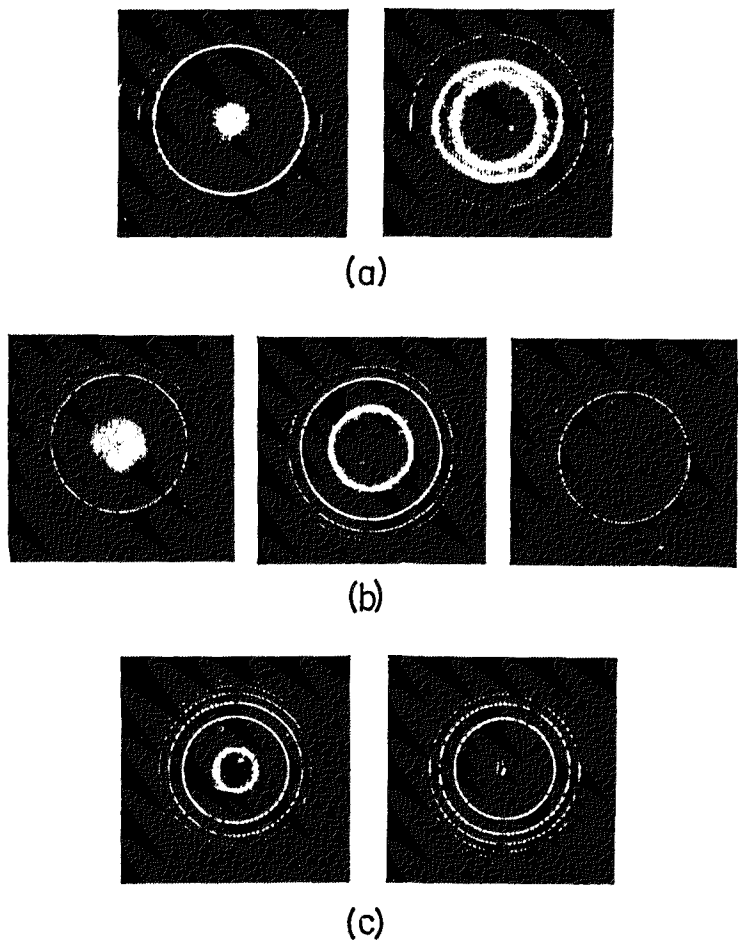

Fig. 13. Typical fringe patterns in the vicinity of confocal separation for a 10-cm FPS. In each case, the source is a single mode He–Ne laser. Variations in the fringe patterns in each horizontal row were obtained by making small changes ($<\lambda/4$) in the mirror separation. (a) $\epsilon = -70\,\mu$, (b) $\epsilon = 0$, (c) $\epsilon = 70\,\mu$.

10, the lens at one end of the instrument serves either of two functions: to direct an incident beam of radiation into the center of the FPS etalon (scanning or filter modes of operation), or to image the interference fringe pattern at infinity when light is incident on the other end of the instrument (visual or photographic modes of operation). In the scanning mode, a small photodetector is mounted directly behind the FPS. We have used both a silicon photodiode and a photomultiplier as the detector (the majority of the scans shown in Sec. III.E were obtained with a photodiode operating in the photovoltaic mode). Since it is desirable—for ease in alignment—to rotate the entire instrument about the entrance aperture, the mounting flange can be attached at either end of the instrument. This flange then serves to attach the instrument to a mirror-mount which is adjustable in angle.

The mirror radius in the FPS is 5 cm, with a corresponding free spectral range of 1500 MHz.* Using multilayer dielectric mirrors, we can obtain a finesse of greater than 150 over a spectral range of about 1200 Å, and with an instrumental transmission of 40% to 45% (compared with the maximum of 50% in the nonmode-matched configuration). With careful mode matching, the instrumental transmission goes to 80–90%, the free spectral range becomes 3000 MHz, and the finesse is doubled—leaving the resolving power unchanged. With broadband multilayer mirrors, a finesse of 150 can be maintained from about 4900 Å to 7000 Å, with an instrumental transmission of approximately 25% (or 50% when mode matched). With these mirrors, this instrument has been used for high resolution spectroscopy with argon lasers (4880 Å and 5145 Å), He–Ne lasers (6328 Å) and Q-switched ruby lasers (6943 Å). A variety of experimental data is shown in Sec. III.E.

In the scanning mode, the instrument is very easy to align to the incident beam of light. First of all, the instrument is located so that the incident light beam (preferably, but not necessarily, more or less collimated) falls close to the center of the lens. The axis of the instrument is then roughly aligned with the incident beam. This can be done most conveniently by observing the light that has been reflected from the FPS back towards the source: the reflected beam should be adjusted to lie fairly close to the incident beam. At this point a high resolution scan display can be observed by monitoring the detector output at an oscilloscope. The display is peaked by further small adjustments to the alignment. The scanning voltage is conveniently provided by the sawtooth (or horizontal scan) voltage from the oscilloscope. This voltage will typically scan two or three free spectral ranges, and assures synchronism between the applied scanning voltage and the oscilloscope sweep. Moreover, this technique provides a highly linear display of the optical spectrum at the oscilloscope.

To observe interference fringes, the detector is removed and the incident beam is directed towards the end of the instrument at which the detector was located. The fringe pattern can then be viewed directly through the lens, or an auxiliary telescope can be used. The latter is particularly useful when the incident beam is not collimated, resulting in a displacement of the plane of the fringe pattern away from the focal plane of the lens. The proper alignment of the instrument axis relative to the incident beam of light can be made by observing fringe pattern and making angular adjustments to make the fringes circular. As mentioned earlier, it may be desirable to change the mirror spacing slightly to obtain a more nearly linear display of frequency in the fringe pattern, although this entails a reduction in the realizable spectral resolution (Fig. 14).

D. Alignment Procedures

In assembling and using FPS interferometers, only a few alignments or adjustments are required, and in this section procedures for these are briefly described.

Note added in proof: By replacing the 5-cm radius mirrors with 1-cm mirrors, and modifying one mirror cell to provide for a 1-cm mirror separation, we were recently able to extend the free spectral range of this instrument to 7.5 GHz (or 0.09 Å at 6000 Å). Using narrowband mirrors, a finesse in excess of 100 was easily attained with a 0.5-mm detector aperture. This type of instrument has proved useful in examining ion laser spectra. Comparable finesse in an FPP with the same free spectral range is very difficult to obtain.

1. *Establishing the Confocal Mirror Separation*

We have pointed out that optimum performance of an FPS depends critically upon the proper spacing of the mirrors. Connes has described an imaging technique for approximating this adjustment which requires only a small incoherent light source.[2] If a He–Ne laser is available, the alignment can be made with high precision as follows. First, adjust the mirror separation to within a millimeter or so from knowledge of the mirror radii. Then, set up the FPS etalon so that a quasi-collimated beam from the gas laser is incident on one mirror, and arrange to view the interference fringes which are formed in the vicinity of the central plane of the etalon. The laser beam diameter should be large enough to allow several fringes to be seen. Next, make a fine adjustment of the mirror separation to bring the mirrors *closer together* by a fraction of a wavelength, and observe the resulting change in the central fringe radius. This fine adjustment can usually be made by manually squeezing the etalon. If the mirror separation is *greater* than the confocal separation, the central fringe will become *smaller* in diameter as the mirrors are moved towards each other. If the mirror separation is *less* than the confocal spacing, the central fringe diameter will *increase* as the mirrors are moved towards one another. Figure 13 shows the appearance of the central fringes on either side of exact confocal spacing, as well as at the confocal spacing. As shown in Fig. 13(a), when the mirrors are spaced by slightly less than confocal spacing, there is a zone [radius $(-2\epsilon r)^{\frac{1}{2}}$] of high dispersion toward which all fringes gravitate as the mirror spacing is slightly reduced (or, equivalently, as the wavelength of the quasi-monochromatic light source is increased). This zone approaches the center of the fringe pattern as the mirror separation is increased, and disappears through the center of the pattern when the confocal spacing is exceeded. The location of this zone is an extremely sensitive indication of the mirror separation, and when the mirrors are exactly confocal it is at the center of the fringe pattern. The radius of this zone, as a function of mirror separation, is shown by the dotted line in Fig. 3.

If the FPS is set up in the scanning mode it is possible to peak up the adjustment of the mirror separation merely by maximizing the amplitude of a displayed laser spectrum while at the same time minimizing the apparent width of individual spectral components. With very little practice it becomes a simple matter to establish confocal separation to within a micron or so using this technique. As the optimum mirror separation is approached, one should also make fine adjustments to the angular alignment—unless a very small diameter beam is used, in which case the spectral display is relatively insensitive to alignment.

2. *Selecting the Optimum Detector Aperture*

As mentioned earlier, the diameter of the detector aperture [or, equivalently, the diameter of the incident beam: see Fig. 10(a)] serves to define both the actual instrumental bandwidth and the étendue. As a rule, one seeks a compromise in which a considerable étendue can be attained with only slight sacrifice in resolving power. The curves in Fig. 8(d) show that the optimum compromise occurs when the radius of the detector aperture (assuming it to be located adjacent to the rear interferometer mirror) is just under ρ_s. Figure 14 shows experimental data for the instrument profile of a 10-cm FPS, with a nominal finesse of just over 100, for various detector apertures. In this figure the desirability of using the optimum detector aperture is obvious. For larger apertures, the *peak* transmitted power goes up very little, and the resolution goes down. Note, however, that at larger apertures more *total* light is transmitted: this may be an important consideration in applications involving weak light sources. It is worth pointing out that the finite time constant of a high finesse FPS precludes the use of very high sweep speeds without suffering a loss in resolution—in this case, too, it would make sense to use a somewhat larger detector aperture than normal.

3. *Alignment for Mode Matching*

There are undoubtedly applications where it might prove useful to extend the free spectral range of an FPS by mode matching. The gain in free spectral range is accompanied by a twofold increase in both finesse and instrumental transmission, so that there is no loss in spectral resolution. There is, however, a very great reduction in the tolerance of the alignment between the FPS axis and the incident light beam, and there is also the restriction that the incoming beam match a lowest order transverse mode of the cavity. This latter restriction is less severe than it might be, due to the degeneracy of a confocal cavity. Unlike a general curved mirror cavity, the position of the beam waist of the lowest order transverse mode is not uniquely de-

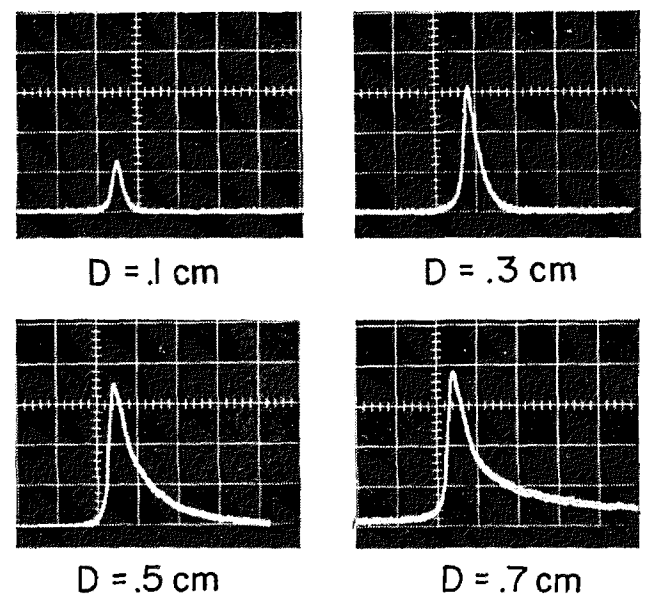

Fig. 14. Observed instrumental profiles for different detector aperture diameters D. Light source was a 1-cm wide collimated single mode laser beam. ($\epsilon \sim 0$; $r = 10$ cm.) The 0.3-cm aperture is clearly the best compromise between signal amplitude and resolution.

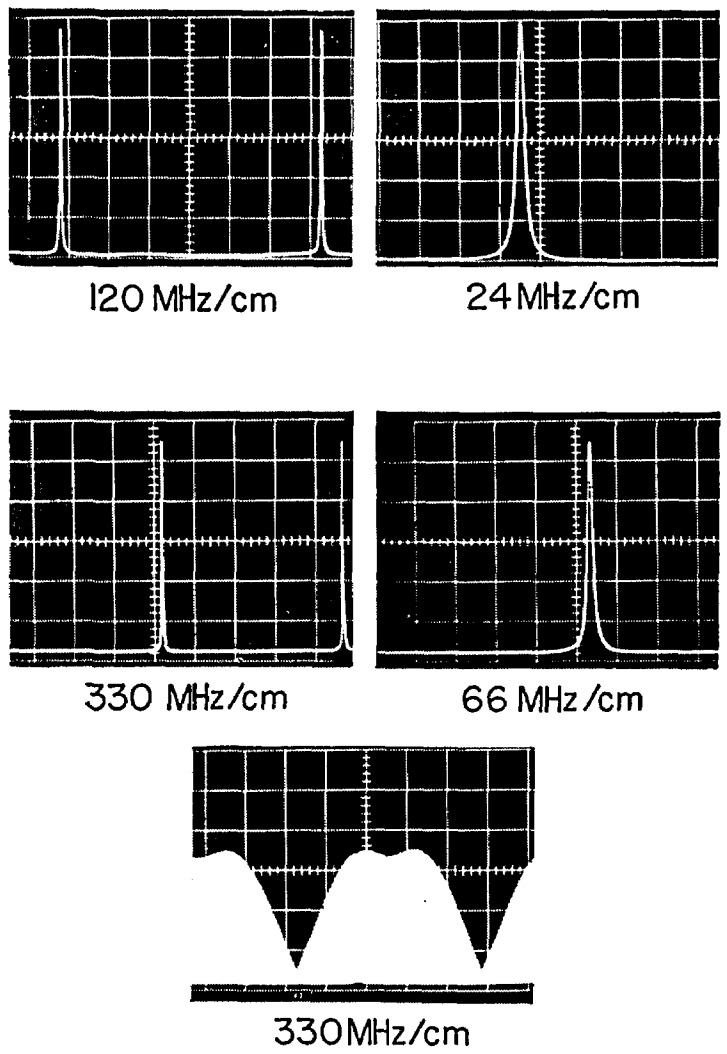

Fig. 15. Spectra of a single mode laser obtained with 5-cm and 10-cm scanning FPS instruments. Top: 10-cm FPS, measured finesse $F \sim 154$; middle: 5-cm (broadband mirrors), $F \sim 148$; bottom: single mode He–Ne gain profile, showing Lamb's dip (see text).

termined, but can be located anywhere between the two mirrors (the diffraction losses are minimized, however, when the beam waist is at the center of the cavity). This type of confocal cavity degeneracy is particularly clear from the geometrical construction for gaussian mode propagation described by Laures.[8] Thus, for a confocal laser, the problem of mode matching is largely a problem of aligning the optical axis of the FPS, i.e., the line joining the centers of curvature of the two mirrors, to that of the incoming light beam. Stated in another way, the basic problem is to locate the source (or its image) and both centers of curvature on a single straight line.

The mode matching alignment problem, as just stated, obviously requires both angular and lateral displacements of the FPS—regarding the source as fixed. When the source is at infinity (collimated), however, it is clear that only angular adjustments are required. This simplifies the problem considerably. Using a collimated beam, the procedure is as follows. First, set up the FPS in the same manner used for observing multiple beam interference fringes [Fig. 10(c)]. Then, while viewing the fringe pattern, adjust the angular alignment of the FPS until a two-beam interference pattern of straight fringes can be seen superimposed on the circular fringes [cf., Fig. 9(a)]. Next, make fine adjustments to increase the straight-fringe spacing until it is large compared to the spot size ρ_s, or at least greater than the detector aperture at the center of an image of the circular fringe pattern. Finally, observe the scan display and touch up the alignment as required. The procedure is somewhat inefficient in that much of the light in the collimated beam fails to reach the detector. Note that the alignment precision is approximately λ/ρ_s and thus requires interferometric stability between the source and the FPS.

As an alternate procedure, one can use the technique described by Fork *et al.* for mode matching to a general curved mirror cavity.[6] Also, we have found that with practice one can set up the FPS in the normal scanning mode and then hunt for the mode-matched condition by making small lateral and angular adjustments while observing the scan display. As the proper alignment is approached, the spectral display in every other free spectral range is slightly increased in amplitude, while the remaining portion of the display is decreased in amplitude. This hunting procedure is not very reliable, and generally takes longer than the alignment described above.

E. Some Experimental Results

One of the first characteristics of an FPS instrument which one would like to determine experimentally is its instrumental bandpass or, equivalently, its finesse. This is conveniently accomplished by observing the spectrum of a relatively stable gas laser, whose individual spectral components are generally orders of magnitude narrower than one could hope to observe directly. Figure 15 shows spectra of a stable single mode He–Ne laser which were obtained with 5-cm and 10-cm scanning FPS instruments of the type described in Sec. III.C. The 5-cm FPS had broadband mirrors (4800 Å to 6900 Å), while the 10-cm FPS had conventional narrowband mirrors peaked at approximately 6500 Å. The finesse in both cases was about 150. The scanning voltage was supplied directly from the oscilloscope's horizontal sweep, and the duration of each sweep was 10 msec. Also shown in Fig. 15 is the gain profile of the single mode He–Ne laser, clearly showing Lamb's dip and thereby the collision-broadened homogeneous linewidth in He–Ne (this gain profile was obtained by slowly changing the laser cavity length and integrating the displayed spectrum with a storage oscilloscope).

We also found that it was a simple matter to indirectly determine the instrumental linewidth by making a direct measurement of the FPS cavity lifetime τ:

$$\tau = 2rF/\pi c = (2\pi\Delta\nu_m)^{-1}. \tag{43}$$

This lifetime could be observed with fair precision by using a 10-nsec Q-switched laser pulse as a realizable approximation to a temporal delta function, and detecting the transmission of the FPS as a function of time with a fast phototube and scope. The resultant trace was very nearly an exponential decay, and gave results in good agreement with other measurements. Note that it is not necessary that the Q-switched pulse have a narrow spectrum, although the alignment between the laser beam and FPS must be good.

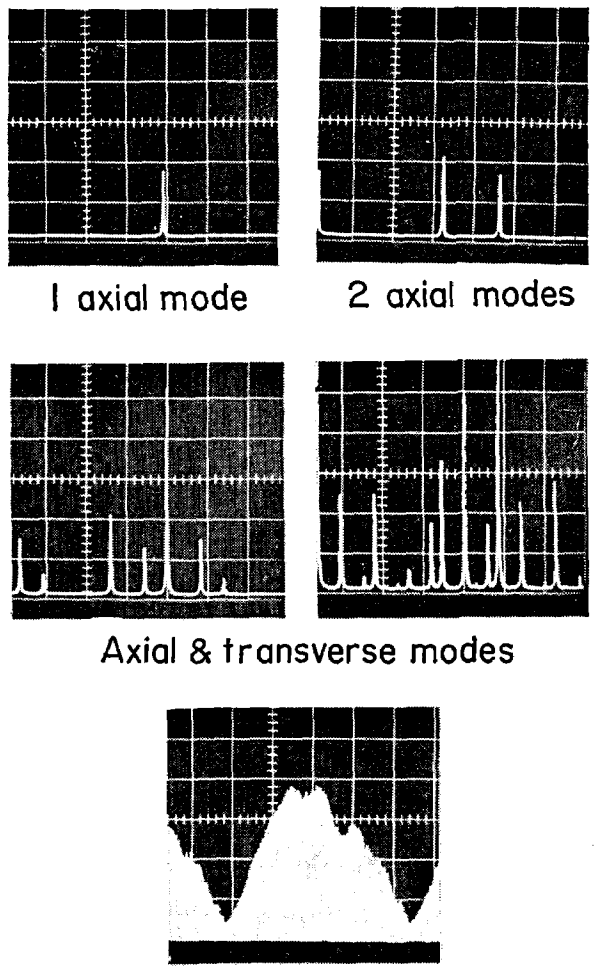

Fig. 16. Spectra of an adjustable multimode He–Ne gas laser. Various numbers of modes were excited by adjusting the laser mirrors. The 5-cm FPS shown in Fig. 12 was used. 330 MHz/cm.

Figure 16 shows the spectra which were obtained using an inexpensive commercially available He–Ne laser which could be operated in one or many transverse and axial modes by adjusting the mirror alignment. This figure clearly shows the ability of the FPS to record the spectra of higher order transverse modes (only by observing the laser spectrum can very weak higher order transverse modes be detected). The gain profile shows a raggedness due to competition effects between different modes, and an asymetry due to the presence of more than one isotope of neon in the He–Ne mixture. The spectra shown in Fig. 16 were all obtained with a 5-cm FPS with a free spectral range of 1500 MHz (or approximately 0.02 Å at 6328 Å).

The fringe patterns shown in Fig. 17(a) and (b) show the spectra of a 60-cm He–Ne laser operating in three axial modes, with just the TEM_{00} transverse mode [see Fig. 17(a)], and with both TEM_{00} and TEM_{01} transverse modes [see Fig. 17(b)]. These spectra were obtained with the same instrument used in obtaining the spectra shown in Fig. 16, although a different laser was used. The mirror separation was approximately 50 μ in excess of confocal, resulting in a lower radial dispersion near the center of the pattern than would otherwise be obtained. Figure 17(c) shows the spectrum of a Q-switched laser operating in a single mode (TEM_{00q}), and was obtained with a 10-cm FPS in exact confocal adjustment. The anomalously large recorded linewidth (>200 MHz) is due to a continuous frequency drift during the evolution of the 10-nsec Q-switched laser pulse. The origin of the frequency drift has not been clearly established, but it is power dependent and approaches zero near threshold for the Q-switched ruby laser.

In many instances it is desirable to make a precise determination of the separation of two spectral lines or of the width of a single line, from a photograph of an FPS fringe pattern. This requires an exact knowledge of both the magnification M of the fringe pattern in the photograph and the departure from confocal separation ϵ. If the two spectral lines in question give rise to fringes of radii ρ_1 and ρ_2 in the photograph of the fringe pattern (both in the same free spectral range), then it is straightforward to show that their frequencies differ by:

$$\Delta\nu \equiv (\nu_2 - \nu_1) = (\bar{\nu}/4r^4)[(\rho_2^4 - \rho_1^4)M^{-4} + 4r\epsilon(\rho_2^2 - \rho_1^2)M^{-2}] \quad (44)$$

where $\bar{\nu}$ is the mean optical frequency. By the same token, if a single spectral component gives rise to fringes of radii ρ_1, ρ_2, and ρ_3 in adjacent free spectral ranges (corresponding to spectral lines of known frequency difference, $c/4r$), then the equation above can be used to solve for both M and ϵ in terms of ρ_1, ρ_2, ρ_3, and r (the mirror radius).

IV. Summary

We have found the spherical Fabry-Perot interferometer to be an extremely versatile high resolution spectroscopic tool. It is particularly well suited, because of its high resolution and limited, free spectral range, to the study of laser and laser-derived, e.g., stimulated and spontaneous scattering of laser light, light sources. It can readily be adapted for pressure or

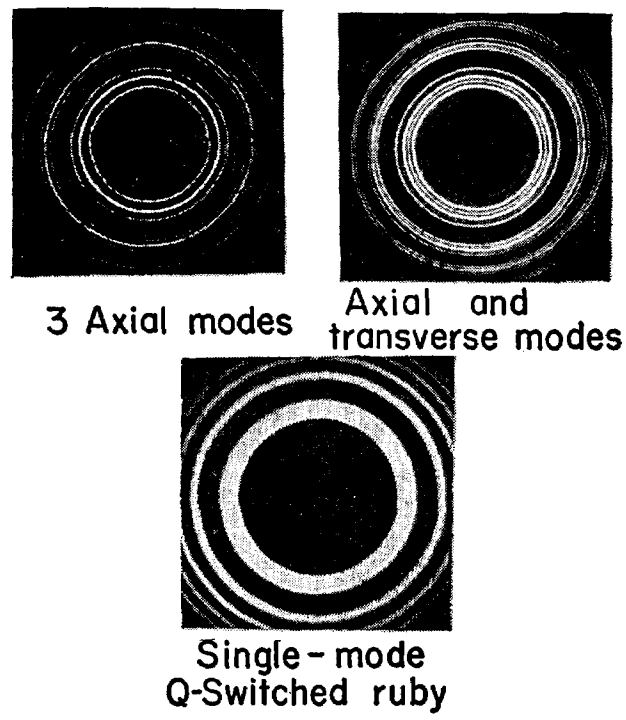

Fig. 17. Top left: spectrum of a He–Ne gas laser operating in three axial modes and the TEM_{00} transverse mode. ($\epsilon \sim 20$ μ, $r = 5$ cm, free spectral range 1500 MHz). Top right: same as above, but with an additional TEM_{01} mode in oscillation. Bottom: spectrum of a 10-nsec single mode pulse from a Q-switched ruby laser (see text). ($\epsilon \sim 0$, $r = 10$ cm, free spectral range 750 MHz).

mechanical scanning, fringe display, or tunable narrow band filtering. The important limitations of an FPS are its relatively narrow free spectral range (generally less than a few thousand megahertz), and the inability to vary the free spectral range attainable with a given pair of mirrors. Some of the advantages of an FPS over other types of optical spectrum analyzers are listed below.

(a) Ease in attaining high finesse—thereby taking advantage of the high reflectivities now available with commercially available dielectric coatings.

(b) Ease of alignment: once the initial mirror separation is set, no further adjustments are required. The only alignment required is that of the entire FPS etalon relative to the light source, and this alignment is not critical.

(c) High étendue (light gathering power) without sacrifice in spectral resolution.

(d) Large acceptance angle when used as an optical filter ($\Omega \approx 4\pi(\lambda/rF)^{\frac{1}{2}}$ sr).

(e) The transverse mode degeneracy of the confocal cavity obviates the necessity for mode matching.

(f) Versatility: a single FPS instrument can be designed to serve in three modes of operation, i.e., scanning, fringe display, and optical filtering.

Using readily available mirror coatings, passive FPS interferometers of reasonable length (50 cm) can easily resolve down to a fraction of a megahertz and, if properly stabilized and thermally compensated, can provide convenient and portable secondary optical wavelength standards. In addition to spectroscopic applications, we plan to use FPS instruments as optical FM discriminators, and as passive elements in laser frequency stabilization servo loops.

Appendix I. Normalized Equations for FPS

In illustrating the performance of an FPS with the calculated curves shown in various figures, we chose to use specific values for the pertinent parameters r, ϵ, λ, and ρ. This was done, rather than using dimensionless normalized parameters, so the reader could get an idea of the actual values of these parameters in a typical case: namely, $r = 10$ cm and $\lambda = 6250$ Å ($\nu = 4.8 \times 10^{14}$ Hz).

If we wish, we can define normalized dimensionless variables; $r_n = r/\lambda$, $\epsilon_n = \epsilon/\lambda$, and $\rho_n = \rho/\lambda$, so that the normalized fringe radii are given by:

$$(\rho_n{}^4 r_n{}^3) + (4\epsilon_n\rho_n{}^2/r_n{}^2) = (m - \xi), \tag{A1}$$

where ξ is the fractional order of interference on axis. The spot size has a normalized radius,

$$(\rho_s)_n = (r_n{}^3/F)^{\frac{1}{4}}. \tag{A2}$$

With these equations, it is straightforward to convert the calculated curves to normalized curves which apply to any set of system parameters. As an alternative, we list below recipes for converting the calculated curves so that they may be used with different values of r and/or λ. (The distances r_0 and λ_0 are 10 cm and 6.25×10^{-5} cm, respectively.)

Figure 3. If the mirror radii are each $r = ar_0$, and if $\lambda = b\lambda_0$, then: (i) change each value of ρ to $\rho' = \rho a^{\frac{1}{2}}$, and (ii) change each value of m, the order of interference relative to the order on axis, to $m' = m/(ab)$, (iii) The ϵ axis remains unchanged. [Note that the curve defining ρ_s corresponds to $m = (1/F)$.]

Figure 4. If $r = ar_0$ and $\lambda = b\lambda_0$, then change ρ to $\rho' = a^{\frac{3}{4}}b^{\frac{1}{4}}\rho$.

Figure 5. If $r = ar_0$ and $\lambda = b\lambda_0$, then: (i) change ρ to $\rho' = a^{\frac{3}{4}}b^{\frac{1}{4}}\rho$, and (ii) change $(\nu - \nu_0)$ to $(\nu - \nu_0)' = (\nu - \nu_0)/a$.

Figure 8. Same as Fig. 4.

References

1. P. Connes, Rev. Opt. **35**, 37 (1956).
2. P. Connes, J. Phys. Radium **19**, 262 (1958).
3. P. Connes, in *Quantum Electronics and Coherent Light* P. A. Miles, Ed. (Academic Press, Inc., New York, 1964), p. 198ff.
4. W. H. Steel, *Interferometry* (Cambridge University Press, Cambridge, 1967), p. 123.
5. K. M. Baird and G. R. Hanes, in *Applied Optics and Optical Engineering*, R. Kingslake, Ed. (Academic Press, Inc., New York, 1967), Vols. 4 and 5, p. 350.
6. R. L. Fork, D. R. Herriott, and H. Kogelnik, Appl. Opt. **3**, 1471 (1964).
7. G. D. Boyd and J. P. Gordon, Bell Sys. Tech. J. **40**, 453 (1961).
8. P. Laures, Appl. Opt. **6**, 747 (1967).